

Four nearby L dwarfs

I. Neill Reid

Dept. of Physics & Astronomy, University of Pennsylvania, 209 S. 33rd Street,
Philadelphia, PA 19104-6396; e-mail: inr@herschel.physics.upenn.edu

J. Davy Kirkpatrick

Infrared Processing and Analysis Center, 100-22, California Institute of Technology,
Pasadena, CA 91125

J. E. Gizis

Department of Physics and Astronomy, University of Massachusetts, Amherst, MA 01003

C. C. Dahn, D. G. Monet

U.S. Naval Observatory, P.O. Box 1149, Flagstaff, AZ 86002

Rik J. Williams

Department of Astronomy, MSC 152, California Institute of Technology, Pasadena, CA
91126-0152

James Liebert

Steward Observatory, University of Arizona, Tucson, AZ 85721

A. J. Burgasser

Dept. of Physics, 103-33, California Institute of Technology, Pasadena, CA 91125

ABSTRACT

We present spectroscopic, photometric and astrometric observations of four bright L dwarfs identified in the course of the 2MASS near-infrared survey. Our spectroscopic data extend to wavelengths shortward of 5000\AA in the L0 dwarf 2MASSJ0746+2000 and the L4 dwarf 2MASSJ0036+1840, allowing the identification of absorption bands due to MgH and CaOH. The atomic resonance lines Ca I 4227\AA and Na I $5890/5896\text{\AA}$ are extremely strong, with the latter having an equivalent width of 240\AA in the L4 dwarf. By spectral type L5, the D lines extend over $\sim 1000\text{\AA}$ and absorb a substantial fraction of the flux emitted in the V band, with a corresponding effect on the (V-I) broadband colour. The KI resonance doublet at $7665/7699\text{\AA}$ increases in equivalent width from spectral type M3 to M7, but decreases in strength from M7 to L0 before broadening substantially at later types. These variations are likely driven by dust formation in these cool atmospheres.

Subject headings: stars: low-mass, brown dwarfs; stars: luminosity function, mass function; Galaxy: stellar content

1. Introduction

Familiarity with one's immediate neighbours is, in general, good policy. In the case of the Solar Neighbourhood, our knowledge of the local constituents forms the basis of the determination of fundamental statistical quantities such as the luminosity function, the mass function, the local mass density and the star formation history of the disk. Moreover, as the apparently-brightest members of their respective spectral classes, the nearest celestial neighbours are most accessible to detailed astrophysical analysis. The latter consideration is of particular importance for objects of intrinsically low luminosity, such as old, low-temperature white dwarfs and ultracool, very low-mass (VLM) main-sequence dwarfs.

Until recently, the main resource for the identification of VLM dwarfs remained the proper motion catalogues compiled by Luyten from photographic material obtained in the 1950s and 1960s using the Palomar 48-inch Oschin Schmidt. The development of higher-sensitivity red and photographic-infrared emulsions in the 1970s permitted photometric surveys to extend to somewhat larger depths, but this field of study has been revolutionised through the advent of deep, near-infrared all-sky surveys, such as DENIS (Epcstein et al, 1994) and 2MASS (Skrutskie et al, 1997). Follow-up observations of sources with extremely red JHK or optical-to-infrared (RIJHK) colours (Delfosse et al, 1997; Kirkpatrick et al, 1999a, hereinafter paper I) have resulted in the identification of numerous ultracool dwarfs. Many are spectroscopically similar to the previously-unique white dwarf companion, GD 165B, which has been transformed from an anomaly to a prototype. The far-red optical spectra of these dwarfs are characterised by the disappearance of TiO and VO absorption bands, the defining signature of spectral class M, and the presence of metal hydride (CaH, FeH, CrH) bands and neutral alkali (Cs, Rb, sometimes Li) lines. The progression of those features was ordered in paper I to define a new spectral class, type L.

The initial sample of ultracool L dwarfs discovered by 2MASS (20 objects) and other surveys (5 dwarfs) includes only two objects with magnitudes brighter than $K=12$: Kelu 1 (Ruiz et al, 1997) and 2MASSJ1439284+192915. As a result, apart from Ruiz et al's observations of Kelu 1, spectroscopy of these sources has been confined largely to wavelengths longward of 6400\AA . We have since extended the areal coverage of our 2MASS

analysis by almost a factor of three, concentrating on identifying late-type L dwarfs. Our current sample includes 74 spectroscopically-confirmed L dwarfs (Kirkpatrick et al, 1999b, hereinafter Paper II). Four (including 2MASSJ1439284+192915) are of particular interest, since their properties imply that they lie at distances of no more than 15 parsecs. All are sufficiently bright that they supply an opportunity of extending high signal-to-noise observations to bluer wavelengths and to higher spectral resolution. This paper provides a brief discussion of the properties of these ultracool dwarfs.

2. Observations

The four L dwarfs discussed in this paper were all identified as candidate low-temperature objects based on analysis of JHK_S photometric catalogues derived from the Two-Micron All-Sky Survey (Skrutskie et al, 1997). 2MASSWJ1439284+192915 forms part of the original L dwarf sample discussed in Paper I; 2MASSWJ0746425+200032 was selected amongst a sample of candidate bright, ultracool late-type dwarfs (discussed further by Gizis et al, 1999); 2MASSWJ0036159+182110 and 2MASSWJ1507476-162738 were identified as likely to be mid- to late-type L dwarfs based on their having (J-K_S) colours redder than 1.3 magnitudes. For brevity, we shall refer to these sources as 2M0036, 2M0746, 2M1439 and 2M1507 throughout the rest of this paper. The individual photometric measurements of each object are listed in table 1: 2M0036 and 2M1507 fall in overlap regions between separate scans and the JHK_s magnitudes are averages of the two observations. A finding chart for 2M1439 is available in Paper I, and finding charts for the other three dwarfs are presented in Paper II.

2.1. Spectroscopy

Each L dwarf has been observed using the Low Resolution Imaging Spectrograph (Oke et al, 1995) on the Keck II telescope. Initial observations were obtained using a 1-arcsecond slit and the 400 l/mm grating blazed at $\lambda 8500\text{\AA}$, covering the wavelength range 6300 to 10200 \AA at a resolution of 9 \AA . An OG570 filter was used to eliminate second-order flux. This is the standard instrumental set-up used in our L dwarf observations, and data reduction and calibration followed the procedures described in paper I. The UT dates of the individual observations were 14 & 16 Dec 1998 (2M0036), 24 Dec 1998 (2M0746), 8 Dec 1997 (2M1439) and 24 Dec, 1998 (2M1507). 2M0746 was also observed on Dec 4, 1998 using the modular spectrograph on the Las Campanas Observatory Du Pont 2.5-metre (see Gizis et al, 1999 for further details), while the 2M1439 observations are described in Paper

I. Spectral types have been derived for each dwarf based on the LRIS spectra plotted in figure 1 following the precepts given in paper I (see Kirkpatrick et al, in prep. for further details).

We have supplemented these intermediate-resolution red spectra with a range of other observations.

LRIS: blue spectra

We also have shorter-wavelength LRIS observations of 2M0036, 2M0746 and 2M1507, using the 300 l/mm grating blazed at 5000Å. Those spectra were obtained on 25 Dec, 1998 (2M0036), 5 March, 1999 (2M0746) and 17 July, 1999. The respective exposure times were 1800, 1800 and 3600 seconds respectively. As with the standard far-red observations, we used a 1-arcsecond slit, providing a spectral resolution of $\sim 6\text{Å}$ and wavelength coverage from ~ 3900 to 7800Å . No order-sorting filters were employed. The data reduction procedures mirror those used in analysing the red data, with flux calibration provided through observations of Hiltner 600 and LTT 9491 (Hamuy et al, 1994). We also obtained lower-resolution data covering the 5400 to 10400Å region for 2M1507 using a 158 l/mm grating on the red channel of double spectrograph on the Hale 200-inc (5.08 metre) telescope. Those data are consistent with the higher signal-to-noise Keck spectrum.

Figure 2 plots the reduced spectra, where we include, for comparison, our observations of the late-type M dwarf BRI0021-0214 (M9.5, Kirkpatrick et al, 1995) and data for the L2 dwarf, Kelu 1 (Ruiz et al, 1997). The latter spectrum was kindly made available by S. Leggett. Figure 3 provides an expanded view of the 4500 to 6600Å region. The more prominent molecular and atomic features are labelled in both figures. Note, in particular, the increasing strength of both the potassium 7665/7699 and sodium 5890/5896 resonance doublets as one progresses from spectral type M9.5 to L5.

HIRES observations

Finally, we have obtained higher-resolution echelle spectra of all four L dwarfs using HIRES (Vogt et al, 1994) on the Keck I telescope. The observations were obtained 24 Aug 1998 (2M0036, 2M1439), 6 March 1999 (2M0746) and 14 June, 1999 (2M1507). In each case, the data provide partial coverage of the wavelength range $\lambda\lambda 6000 - 8500\text{Å}$, including important features such as Li I 6708Å, K I 7665/7699Å, Rb I 7800 & 7948Å, and the Na I 8183/8195Å doublet. Total exposure times of 6000 seconds were accrued on each source. As discussed further below, lithium was not detected in any of these four L dwarfs.

The HIRES data were flat-field corrected and the spectra extracted using programmes written by T. Barlow. The wavelength calibration, based on Th-Ar arc lamp exposures, was

determined using the iraf routines ECIDENTIFY and DISPCOR. We have not attempted to set these data on a flux scale. Radial velocities were computed for each star either from the measured wavelength of the H α emission line (in 2M0746 and 2M1439) or by measuring the central wavelengths of atomic lines due to Cs and Rb, adopting heliocentric corrections given by the IRAF RV package. Our radial velocity measurements for M dwarfs from the Marcy & Benitz (1989) sample indicate that the latter technique can give velocities accurate to $\pm 1.5 \text{ kms}^{-1}$. However, the atomic lines are relatively broad in the L dwarfs, and an internal comparison of the individual measurements suggests that the uncertainty is 2-3 kms^{-1} . Save for 2M1439, the uncertainties in the derived space motions are dominated by the parallax measurements.

2.2. Photometry

CCD images in several passbands have been obtained of all four L dwarfs discussed in this paper. The observations were made using the 40-inch telescope at the Flagstaff station of the US Naval Observatory. Full details of the data reduction and calibration process are given by Dahn et al (in prep.). Those data are listed in Table 1.

In addition to these direct measurements, we have used the calibrated spectra plotted in figures 1 and 2 to synthesise (B-V), (V-R) and (V-I) colours. As in Paper I, square passbands are adopted for each filter, and the flux zeropoints are those of the Johnson/Kron-Cousins system (Bessell, 1979). In general, there is reasonable agreement between the spectroscopic colours and the available direct measurements.

Finally, we have estimated bolometric magnitudes for each dwarf. While none of these sources, and relatively few late-type M or L dwarfs in general, have observations at wavelengths longward of $2.2\mu\text{m}$, the available data suggest that m_{bol} can be inferred with reasonable accuracy from the observed magnitude at the $1.25\mu\text{m}$ J band. Leggett et al (1996) infer $BC_J = 2.07$ magnitudes for the M6.5 dwarf GJ 1111; Tinney et al (1993) infer $BC_J = 1.7$ mag for the L4 dwarf GD165B; and Leggett et al (1999) have derived $BC_J = 2.19$ mag for Gl 229B. These results indicate that there is relatively little variation in BC_J over this temperature range ($\sim 2700\text{K}$ to $\sim 950\text{K}$) and we have adopted a uniform correction of $M_{bol} = M_J + 1.75$ mag for each object in the current sample.

2.3. Astrometry

All four L dwarfs discussed in this paper have been placed on the US Naval Observatory (Flagstaff) CCD parallax programme (Monet et al, 1992). Preliminary absolute parallaxes are available in each case, and those data are listed in Table 2. These observations are also used to derive absolute proper motions, and the results for 2M0036, 2M0746 and 2M1439 are listed in Table 2. In the case of 2M1507, the USNO observations span a period of only 107 days, leading to significant uncertainties in μ and θ . Fortunately, that dwarf is visible on both the first and second epoch plates taken by the UK Schmidt telescope as part of the southern sky survey. Most of the L dwarfs listed in paper I are visible on the POSS II IVN I-band plates, and several are also detected on POSS II IIIaF (R-band) plate material. 2M1507 is unusual in that it is sufficiently bright to be detected on even the IIIaJ (blue-green) 1st-epoch UKST plates. The time difference between the two UKST observations is 11 years, sufficient to allow a more accurate estimate of the proper motion than provided by current CCD observations. We have used standard profile-fitting techniques to measure the displacement between the two epochs and derive an annual proper motion close to 1 arcsecond directed almost due south. Note that three of the four L dwarfs have motions consistent with their inclusion in the Luyten Half Second catalogue.

3. Discussion

These new observations allow us to investigate further the spectral energy distribution and atmospheric composition of L dwarfs. In addition, we can determine space velocities for the four objects in the present sample.

3.1. Molecular features

Far-red optical spectra of L dwarfs show that metal hydride bands, notably CaH, FeH and CrH, become increasingly prominent with decreasing temperature (later spectral types). This behaviour is reminiscent of that observed in late-type metal-poor subdwarfs. In both cases, the greater visibility of the hydride bands reflects decreasing strength of TiO and VO absorption, albeit governed by two different mechanisms: in the subdwarfs, the weak oxides are due to an overall scarcity of metals; in the L dwarfs, TiO and VO are depleted as dust particles, mainly perovskite, CaTiO_3 , and solid-phase VO respectively. Other minerals, such as enstatite (MgSi_3) and forsterite (Mg_2SiO_4), are also expected to condense at temperatures between $\sim 2100\text{K}$ and 1500K (Fegley & Lodders, 1996; Burrows

& Sharp, 1999; Lodders, 1999).

By analogy with cool subdwarfs, other hydrides are expected to be visible at shorter wavelengths - in particular, MgH (Cottrell, 1978). Figure 4 plots our LRIS observations of three extreme ($[m/H] < -1.5$) dwarfs: LHS 489 (esdM0 on the system defined by Gizis, 1997), LHS 453 (esdM3.5) and LHS 375 (esdM5). Those observations were obtained on 17 July, 1999 using the same instrumental setup and data reduction process as in our observations of 2M1507. Comparing spectra for the two sets of objects reveals both significant similarities and differences. The L dwarfs are substantially cooler than the ~ 3000 to 4000K esdMs, leading to much steeper spectral energy distributions in the former than the latter. In both cases, however, the most prominent molecular absorption is due to metal hydrides, with the 5200\AA MgH feature obvious in all of the L dwarfs. The $\lambda 4788\text{\AA}$ band is clearly present in the L5, 2M1507, and is barely detected in 2M0036.

TiO bands at 4761 , 4954 and 5448\AA are evident in 2M0746, but have disappeared by spectral type L4. All of the L dwarfs also exhibit strong absorption at $\sim 5500\text{\AA}$ with the band most prominent in 2M0746. This feature is likely to be calcium hydroxide, CaOH, originally identified in mid-type M dwarfs by Pesch (1972) and increasingly strong in later-type M dwarfs. This molecule also contributes a diffuse band at $\sim 6230\text{\AA}$ (Pearse & Gaydon, 1965), which is blended with the $\lambda 6158\text{\AA}$ γ' TiO band in M dwarfs (Boeshaar, 1976). The latter two bands are likely responsible for the substantial, double-bottomed absorption feature at $\sim 6200\text{\AA}$ in 2M0746, evident as a shallower depression in the L4, 2M0036. Both CaOH and MgH can be identified in the spectrum of Kelu 1 presented by Ruiz et al (1997). Finally, the VO $\lambda 5736\text{\AA}$ band is probably responsible for a relatively weak absorption feature in 2M0746.

3.2. Atomic lines

Table 3 lists equivalent widths for some of the more prominent atomic lines present in the spectra of these objects. We list results from measurements of both the LRIS spectra plotted in figure 1 and of our HIRES data. The latter provide only incomplete wavelength coverage, but the higher-resolution data allow more accurate measurements of weaker lines. In particular, the Ca I 6572\AA and 8256\AA absorption lines and $H\alpha$ emission are barely detectable in the LRIS spectra, where the measured equivalent widths have a 1σ uncertainty of $\pm 0.5\text{\AA}$.

One of the strongest features, either atomic or molecular, in the far-red spectra of L dwarfs is the K I $7665/7699\text{\AA}$ resonance doublet. Those lines have individual equivalent

widths of 10 to 12 Å at spectral type L0, but increase dramatically in strength with decreasing temperature to the extent that the lines effectively merge at \sim L5, where the composite feature has a width exceeding 100Å. Similarly, the Rb I and Cs I lines show distinctly non-linear behaviour, increasing substantially in strength between the L4 dwarf 2M0036 and 2M1507 (L5).

In paper I we proposed that this behaviour is another consequence of dust formation. As discussed further in section 3.5, dust initially contributes a scattering layer at late-type M dwarfs, but in lower temperature atmospheres (later spectral types) the dust particles either ‘rain out’ to greater depths (below the photosphere) or form larger particles, in either case reducing scattering at optical wavelengths. The overall atmospheric transparency is further increased as metals are transformed to solid phase, both by the removal of TiO and VO molecular absorption, and through the scarcity of free electrons and the resulting reduced level of H^- continuum opacity.

The $\tau = 1$ photosphere lies at a large physical depth within the low opacity L-dwarf atmosphere, with the result that the column density of (relatively) undepleted elements, such as the alkali metals, can reach very substantial values. In addition, gas pressure increases with increasing depth leading to substantial van der Waal’s broadening, as in degenerate white dwarfs. Both effects lead to strong atomic lines. As discussed in paper I, the relative strengths of the resonance lines of those species visible in the far red (K, Cs, Rb) are consistent with their relative abundances in the Sun. (The Ca I 6572Å line and the Na I 8183/8194 doublet are higher-order transitions.) Sodium is not expected to form grains until temperatures of less than 1200K (the T-dwarf régime) and, with a higher abundance than potassium ($[Na] = 6.31$ as compared to $[K]=5.13$ for $[H]=12.0$, where $[m]$ is the logarithmic abundance), the D lines at 5890, 5896Å are predicted to grow in strength at earlier spectral types than the K I doublet.

This prediction is confirmed by the spectra plotted in figures 2 and 3. The sodium lines, which already have the substantial equivalent width of ~ 36 Å in the M9.5 BRI0021 have doubled in strength to ~ 80 Å by spectral type L0.5 (2M0746). We measure an equivalent width of ~ 170 Å in the L2 dwarf Kelu 1, and our spectrum of 2M0036 yields an equivalent width of ~ 240 Å for that L3.5 dwarf, although identifying appropriate pseudo-continuum points is becoming problematic at these later spectral types.

Initial observations of 2M1507 with the Palomar double spectrograph revealed a steeply declining spectrum shortward of 6700Å, with no significant flux detected shortward of ~ 6000 Å. Our surmise that this might reflect increased sodium absorption is confirmed spectacularly by the LRIS data plotted in figure 2. Superimposed on the steeply-rising underlying spectrum, the D lines produce a smooth, concave feature spanning over 1500Å,

with MgH the only identifiable absorption feature between 4500 and 6500Å. The blue wing of this atomic doublet extends to $\sim 5000\text{\AA}$, where the spectral energy distribution reaches a mild peak before declining towards shorter wavelengths. The red wing of the Ca I 4227Å resonance line probably contributes to that smooth decline. Similar behaviour in the K I 7665/7699 doublet at much cooler temperatures is partly responsible for the steep flux gradient between 8000 and 9000Å in the energy distribution of methane-rich T dwarfs such as Gl 229B (Oppenheimer et al, 1998).

3.3. Chromospheric activity and lithium absorption

H α emission has long been known as an indicator of chromospheric activity amongst M dwarfs, and earlier studies suggested that emission became increasingly common amongst later spectral types. Gizis et al (1999), however, have re-examined the distribution of chromospheric activity as a function of spectral types, using 2MASS observations to define a photometrically-selected sample of M dwarfs which includes a significantly larger number of ultracool ($>M7$) objects than was previously available. Analysis of that sample shows that the frequency of H α emission peaks at close to 100% at spectral type M7 and declines thereafter. Only 45% of known early-type ($\leq L3$) L dwarfs have emission lines with equivalent widths exceeding $\sim 2\text{\AA}$ while none of the later-type L dwarfs in paper I have detectable emission, despite the low continuum flux in the latter objects.

The four sources considered here show behaviour similar to the dwarfs in the paper I sample. Both of the earlier-type dwarfs have weak H α emission, while no emission is detectable in the two later-type dwarfs. Figure 5 plots our HIRES data for the H α region of the spectrum in three objects - the 2M1507 data are of low signal to noise at these wavelengths and essentially featureless. Both of the H α profiles, but particularly 2M1439, appear to have a narrow core centred on a broader pedestal. This morphology is also found in approximately 10% of the ultracool M dwarfs.

None of these dwarfs is particularly active. We can use our flux-calibrated LRIS spectra to determine emission line fluxes from our measured equivalent widths. In the case of 2M0746, we derive $F_\lambda \sim 2.6 \times 10^{-16} \text{ erg cm}^{-2} \text{ sec}^{-1}$, while for 2M1439 we find $F_\lambda \sim 7.8 \times 10^{-17} \text{ erg cm}^{-2} \text{ sec}^{-1}$. These correspond to activity ratios, L_α/L_{bol} , of $10^{-5.5}$ and $10^{-5.4}$ respectively, values which are almost two orders of magnitude lower than the typical level of activity amongst M dwarfs, $\langle \frac{L_\alpha}{L_{bol}} \rangle \sim 10^{-3.8}$ (Hawley et al, 1996; Gizis et al, 1999) and an order of magnitude below the quiescent state of the ultracool M9.5e dwarf, 2MASSW J0149090+295613 $\langle \frac{L_\alpha}{L_{bol}} \rangle \sim 10^{-4.6}$ (Liebert et al, 1999). The upper limits corresponding to non-detection imply even lower activity ratios for the two later-type dwarfs.

Our HIRES observations also allow us to set limits on the equivalent width of the Li I 6708Å absorption line in these four dwarfs. The presence of atmospheric lithium in late-type dwarfs is now well-recognised as an indicator of substellar mass (Rebolo et al, 1992; Magazzu et al, 1993). Recent models indicate that all dwarfs with masses exceeding $0.06M_{\odot}$ should have depleted lithium by the time that their surface temperature has fallen to $\sim 2400\text{K}$, equivalent to spectral type M7 (Baraffe et al, 1998). Based on the scale derived in paper I, we estimate temperatures between $\sim 2100\text{K}$ (2M0746) and $\sim 1700\text{K}$ (2M1507) for the four dwarfs considered here. None has lithium absorption exceeding $200\text{m}\text{\AA}$. Approximately one in four of the 80 L dwarfs identified to date from 2MASS data have detectable lithium absorption, with equivalent widths rising to $\sim 20\text{\AA}$ amongst the later spectral types (Kirkpatrick et al, in prep). Thus, the absence of detectable lithium in these dwarfs implies that all of these dwarfs have depleted their primordial store of lithium: that is, all four have masses which exceed $0.06M_{\odot}$.

That these four L dwarfs have masses relatively close to the hydrogen-burning limit is not surprising. Figure 19 in paper I shows the predicted time evolution of temperature for models spanning the mass range 0.01 to $0.1 M_{\odot}$. Both the calculations by Baraffe et al (1998) and Burrows et al (1997) predict that objects with masses as high as $\sim 0.08M_{\odot}$ (i.e. very low mass stars) can achieve temperatures of 2100K , the value we associate with spectral class L0. Similarly, the upper mass limit at $T_{eff} \sim 1700\text{K}$ (L5) is 0.07 to $0.075 M_{\odot}$. In both cases, higher mass objects spend several Gyrs at those temperatures, while brown dwarfs with masses below $\sim 0.06M_{\odot}$ have total residence times of no more than $\sim 10^8$ years. Those circumstances lead to much higher probabilities of detecting high-mass brown dwarfs and very low mass stars at early and mid-L spectral types. Lower-mass brown dwarfs make a larger contribution to samples of late L dwarfs.

3.4. Kinematics

Table 2 shows that all four L dwarfs have substantial velocities relative to the Sun. The correlation between space motion is statistical rather than direct, but since velocity dispersion increases with age, there is less ambiguity in interpreting a high velocity as implying a relatively old age than in taking a low velocity as implying youth. Representative tracers of the ‘young disk’ population (A stars, active late-type dwarfs, Cepheids) indicate that a 1-Gyr old population can be modelled as a Schwarzschild ellipsoid with $[U = -10, V=-10, W=-7; \sigma_U = 38, \sigma_V = 26, \sigma_W = 21 \text{ kms}^{-1}]$ (Soderblom, 1990). The average space velocity for those kinematics is $V_{tot} = 34\text{kms}^{-1}$, and even the lowest velocity L dwarf in the current sample, 2M1507, lies at the 75th percentile of the predicted velocity distribution,

albeit within 1σ of the mean.

The measured velocities are more characteristic of an older stellar population. Hawley et al (1996) derive the following ellipsoid from observations of nearby M dwarfs: [$U = -10$, $V = -21$, $W = -8$; $\sigma_U = 38$, $\sigma_V = 26$, $\sigma_W = 21\text{kms}^{-1}$]. Matched against that distribution, 2M0036, 2M0746, 2M1439 and 2M1507 fall at the 48th, 68th, 93rd and 39th percentiles. It therefore seems unlikely that these dwarfs are younger than ~ 1 Gyr, further corroborating their identification as high-mass brown dwarfs or low-mass stars.

3.5. Colour-magnitude diagrams

Our spectrophotometry provides the first opportunity of examining the BV colours of L dwarfs. It is notable that the (B-V) colour inferred from the spectrophotometry for 2M0036 is ~ 0.5 magnitudes bluer than that for the L0 dwarf, 2M0746. This counter-intuitive blueward evolution with decreasing temperature can be ascribed in large part to the increasing strength of the Na D lines. A complementary effect can be expected in the (V-I) colour.

Figure 6 plots the (M_V , (V-I)) colour magnitude diagram for nearby stars with accurate parallaxes and reliable photometry (Bessell, 1990; Leggett, 1992) supplemented by our own data for the four bright L dwarfs discussed in this paper. 2M1507 has a formal visual absolute magnitude of $M_V \sim 22.9$. Among M dwarfs, (V-I) reaches a local maximum at spectral type $\approx M7$: VB8 (M7) has (V-I)=4.56 mag, while VB10 is only slightly redder at (V-I) ~ 4.7 mag. Later-type M dwarfs, such as LHS 2924 (M9, (V-I) ~ 4.37), have lower luminosities, but bluer (V-I) colours (Monet et al, 1992). Our new data show that the march redward resumes amongst the L dwarfs, with the growing strength of the sodium D lines contributing to the decreased flux in the V band, notably the nearly 1 magnitude offset in (V-I) between 2M0036 (L4) and 2M1507 (L5).

The cause of the reversal in (V-I) colour amongst the later-type M dwarfs has received little discussion in the literature. Spectroscopy shows no evidence for increased molecular absorption in the far red, which might decrease the emergent flux in the I band. Indeed, the strongest molecular absorber, TiO, peaks between $\sim M6$ and M8 (the γ 7050Å band is strongest at M6.5) and decreases in strength in dwarfs of later spectral type, while other species, such as VO, have less extensive absorption bands. These same stars show a near-monotonic trend toward redder colours with decreasing luminosity in optical to infrared colours, such as (I-J) (figure 4). This suggests that the colour reversal in (V-I)

stems primarily from increased flux in the V band rather than a deficit at I-band¹. The (M_J , (I-J)) diagram beautifully illustrates the ‘step’ in the main sequence at spectral type $\approx M4$, originally highlighted by Reid & Gizis (1997) and probably due to the onset of convection. The L0 dwarf 2M0746 lies ~ 0.7 magnitudes above the ‘main sequence’ in this plane, raising the possibility that it is an equal-mass binary.

We suggest that the behaviour the (V-I) colour is driven by the formation of dust in the upper atmospheric layers of mid-type M dwarfs, and by the subsequent evolution of the particle size and/or spatial distribution at lower effective temperatures. Tsuji et al (1996) originally demonstrated that dust formation has an important effect on the emergent spectral energy distribution of cool dwarfs, notably a reduction in the strength of the near-infrared H₂O bands due to atmospheric heating through dust re-radiation. Allowing for the latter effect reconciles a long-standing discrepancy between theoretical models and observations of late-type M dwarfs (cf Reid & Gilmore, 1984). Our hypothesis is that the colour reversal in (V-I) has the same origin.

Tsuji et al (1996) place the onset of dust formation at $T_{eff} \sim 2600\text{K}$. Leggett et al (1996) estimate $T_{eff} \sim 2700\text{K}$ for the M6.5 dwarf GJ 1111, suggesting that dust should become evident at spectral types of $\approx M7$ and later. Supporting evidence for dust formation at this spectral type comes from variations in the equivalent width of the 7665/7699 KI doublet in mid- the late-M dwarfs. Figure 7 plots HIRES data covering this region of the spectrum for eight dwarfs with spectral types between M3 and L4. While the detailed profile of the shorter wavelength component is obscured partially by terrestrial O₂ absorption (the A band), it is clear that the overall variation mimics that of the (V-I) colour. The equivalent widths rise to a maximum at spectral type M6.5/M7, declines noticeably in strength to spectral type M9.5/L0, before increasing dramatically throughout the L dwarf sequence, as discussed above and in paper I.

We explain this behaviour as a combination of two effects. First, at spectral types M7-M9.5, dust is present in the atmosphere in sufficient quantities to act as a scattering layer, raising the atmospheric opacity and hence reducing the physical depth (and hence both gas pressure and column density) of the $\tau = 1$ layer for line formation; second, dust re-radiation not only reduces the strength of the H₂O bands, but also increases the flux emitted at visual wavelengths, resulting in bluer (V-I) colours. Dust formation may also reduce the overall molecular (mainly TiO) opacity to a greater extent at visual wavelengths

¹Note, however, that the growth in strength of the K I 7665/7699Å resonance lines amongst the later L dwarfs is likely to result in an effect on M_I analogous to the effect of the D lines on M_V between spectral types L4 and L5. Gl 229B is almost 1 magnitude redder in (I-J) than the L8 dwarf 2MASSWJ1632291+190441.

than at $0.8\mu\text{m}$. In late M dwarfs, such as LHS 2924, the total flux emitted at visual wavelengths amounts to less than 0.1% of the bolometric flux, so a small flux redistribution can have a large effect on F_V . Section 3.2 summarises the likely explanations for the increased equivalent widths in all of the alkali lines at spectral types beyond L0: increased particle size or rain out. More detailed spectrophotometry of mid- to late-type M dwarfs at blue and visual wavelengths can test the overall validity of this hypothesis.

4. Summary and Conclusions

We have presented spectroscopic and photometric data for four bright L dwarfs lying at distances of less than 15 parsecs from the Sun. Our observations permit the first detailed examination of the properties of these objects at blue and visual wavelengths, revealing the presence of MgH and CaOH molecular absorption. In addition, the sodium D lines are extremely strong, reaching equivalent widths in excess of 240\AA in later-type L dwarfs. This behaviour likely stems from the low atmospheric opacity in the latter objects and the consequent substantial pressure broadening. The growth in strength of the Na D lines is also responsible for the (V-I) colour becoming significantly redder between spectral types L4 and L5. The KI 7665/7699 doublet probably has a similar effect on the I-band flux between spectral types L8+ and T.

Dust formation is clearly an important factor governing spectral evolution at these low temperatures. Theoretical models suggest that dust first forms, primarily as TiO-based agglomerates, at $\sim 2600\text{K}$, a prediction which is supported by the behaviour of the KI lines at 7665/7699 \AA at spectral types between M3 and L0. Indeed, we suggest that the reversal in the (M_V , (V-I)) relation at spectral type $\approx M7$ may be a consequence of both lower molecular opacities and dust re-radiation heating the atmosphere, with a consequent increase in the flux emitted at visual wavelengths.

None of the four L dwarfs considered here has detectable lithium absorption, indicating masses of at least $0.06M_\odot$. All, however, are also chromospherically inactive, implying masses close to, if not below, the hydrogen-burning limit, and the relatively high space motions suggest ages of ~ 1 Gyr or more. Taken together, these indicators suggest masses of from 0.07 to $0.09M_\odot$. Further detailed observations of these and other bright L dwarfs will prove important in determining the general physical characteristics of these objects.

The authors would like to thank Pat Boeshaar for illuminating discussion on the CaOH molecule and Sandy Legget for providing a copy of the blue spectrum of Kelu 1. We would also like to thank the staff of the Keck Observatories for their skilled and enthusiastic

support in acquiring the observations for this project.

JDK, INR and JL acknowledge funding through a NASA/JPL grant to 2MASS Core Project science. AJB and RJW acknowledge support from this grant.

Much of the V,I photometry reported in Sec. 2.2 was obtained by H. Harris as part of the USNO parallax efforts and we thank him for allowing the use of it here. The astrometric data reported in Sec. 2.3 were acquired by a team of observers which includes B. Canzian, H. Guetter, S. Levine, C. Luginbuhl, A. Monet, R. Stone, and R. Walker. We thank them for their contributions.

This publication makes use of data from the 2-Micron All-Sky Survey, which is a joint project of the University of Massachusetts and the Infrared Processing and Analysis Center, funded by the National Aeronautics and Space Administration and the National Science Foundation.

The Keck Observatory is operated by the Californian Association for Research in Astronomy, and was made possible by generous grants from the Keck W. M. Foundation.

This work is based partly on photographic plates obtained at the Palomar Observatory 48-inch Oschin Telescope for the Second Palomar Observatory Sky Survey which was funded by the Eastman Kodak Company, the National Geographic Society, the Samuel Oschin Foundation, the Alfred Sloan Foundation, the National Science Foundation grants AST84-08225, AST87-19465, AST90-23115 and AST93-18984, and the National Aeronautics and Space Administration grants NGL 05002140 and NAGW 1710. JDK and AJB acknowledge the support of the Jet Propulsion Laboratory, California Institute of Technology, which is operated under contract with the National Aeronautics and Space Administration.

REFERENCES

- Baraffe, I., Chabrier, G., Allard, F., Hauschildt, P.H. 1998, *A&A*, 337, 403
- Bessell, M.S. 1979, *PASP*, 91, 589
- Bessell, M.S. 1990, *A&AS*, 83, 357
- Boeshaar, P. C. 1976, Ph. D. thesis, Ohio State Univ.
- Burrows, A., Marley, M., Hubbard, W.B., Lunine, J.I., Guillot, T., Saumon, D., Freedman, R., Sudarsky, D., Sharp, C. 1997, *ApJ*, 491, 856
- Burrows, A., Sharp, C. 1999, *ApJ*, 512, 843
- Cottrell, P.L., 1978, *ApJ*, 228, 544

- Delfosse, X., Tinney, C.G., Forveille, T., Epchstein, N., Bertin, E., Borsenberger, J., Copet, E., de Batz, B., Fouque, P., Kimeswenger, S., Le Bertre, T., Lacombe, F., Rouan, D., Tiphene, D. 1997, *A&A*, 327, L25
- Epchtein, N., De Batz, B., Copet, E. et al 1994, in *Science with Astronomical Near-infrared Sky Surveys*, ed. N. Epchtein, A. Omont, B. Burton, P. Persei, (Kluwer, Dordrecht), p. 3
- Fegley, B., Lodders, K. 1996, *ApJ*, 472, L37
- Gizis, J.E. 1997, *AJ*, 113, 806
- Gizis, J.E., Monet, D.G., Reid, I.N., Williams, R. 1999, *AJ*, submitted
- Hamuy, M., Suntzeff, N.B., Heathcote, S.R., Walker, A.R., Gigoux, P., Phillips, M.M. 1994, *PASP*, 106, 566
- Hawley, S.L., Gizis, J.E., Reid, I.N. 1996, *AJ*, 112, 2799
- Kirkpatrick, J.D., Reid, I.N., Liebert, J., Cutri, R.M., Nelson, B., Beichmann, C.A., Dahn, C.C., Monet, D.G., Gizis, J., Skrutskie, M.F. 1999a, *ApJ*, 519, 802 (paper I)
- Kirkpatrick, J.D., Reid, I.N., Gizis, J.E., Burgasser, A.J., Liebert, J., Monet, D.G., Dahn, C.C., Nelson, B. 1999, *ApJ*, submitted
- Leggett, S.K. 1992, *ApJS*, 82, 351
- Leggett, S.K., Allard, F., Berriman, G., Dahn, C.C., Hauschildt, P. 1996, *ApJS*, 104, 117
- Leggett, S.K., Toomey, D.W., Geballe, T.R., Brown, R.H. 1999, *ApJ*, 517, L139
- Liebert, J., Kirkpatrick, J.D., Reid, I.N., Fisher, M.D 1999, *ApJ*, 519, 345
- Lodders, K. 1999, *ApJ*, 519, 793
- Magazzu, A., Martin, E.L., Rebolo, R. 1993, *ApJ*, 404, L17
- Marcy, G.W., Benitz, K.J. 1989, *ApJ*, 344, 441
- Monet, D.G., Dahn, C.C., Vrba, F.J., Harris, H.C., Pier, J.R., Luginbuhl, C.B., Ables, H.D., 1992, *AJ*, 103, 638
- Oke, J. B., Cohen, J. G., Carr, M., Cromer, J., Dingizian, A., Harris, F. H., Labreque, S., Lucinio, R., Schaal, W., Epps, H., Miller, J. 1995, *PASP*, 107, 375

- Oppenheimer, B.R., Kulkarni, S.R., Matthews, K., van Kerkwijk, M.H. 1998, ApJ, 502, 932
- Pearse, R.W.B., Gaydon, A.G. 1965, *The Identification of Molecular Spectra*, (Chapman & Hall, London)
- Pesch, P. 1972, ApJ, 174, L155
- Rebolo, R., Martín, E.L., Magazzu, A. 1992, ApJ, 389, L83
- Reid, I.N., Gilmore G.F. 1984, MNRAS, 206, 19
- Reid, I.N., Gizis, J.E. 1997, AJ, 113, 2246
- Ruiz, M.T., Leggett, S.K., Allard, F. 1997, ApJ, 491, L107
- Skrutskie, M.F. et al 1997, in *The Impact of Large-Scale Near-IR Sky Survey*, ed. F. Garzon et al (Kluwer: Dordrecht), p. 187
- Soderblom, D.R. 1990, AJ, 100, 204
- Tinney, C.G., Mould, J.R., Reid, I.N. 1993, AJ, 105, 1045
- Tinney, C.G. 1996, MNRAS, 281, 644
- Tsuji, T., Ohnaka, K., Aoki, W. 1996, A&A, 305, L1
- Vogt et al, 1994, S.P.I.E., 2198, 362

Table 1
L dwarf photometry

Name	Sp.	$(B-V)_{SP}$	$(V-R)_{SP}$	V	I_C	J	H	K
2M0036	L3.5	1.7 ± 0.2	3.0 ± 0.1	21.33 ± 0.06	16.10 ± 0.02	12.44	11.58	11.03
2M0746	L0.5	2.1 ± 0.2	2.3 ± 0.1	19.87 ± 0.06	15.11 ± 0.02	11.74	11.00	10.49
2M1439	L1			21.04 ± 0.02	16.12 ± 0.02	12.76	12.05	11.58
2M1507	L5			22.9 ± 0.5	16.65 ± 0.02	12.82	11.90	11.30

Table 2
L dwarf astrometry and kinematics

Parameter	2M0036	2M0746	2M1439	2M1507
μ arcsec yr ⁻¹	0.833±0.073	0.464±0.091	1.2943±0.0012	0.99±.05
θ degrees	80±15	250±2	288.3±0.1	174±5
π milliarcsec	92.2±16.3	69.4±16	69.5±0.6	117.5±25.2
V_{rad} kms ⁻¹	21.7±3.0	56.6±2.0	-23.9±2.0	-36.4±3.0
M_K	10.86±0.35	9.70±0.45	10.70 ±0.02	11.65±0.42
M_{bol}	14.00	12.70	13.65	14.90
U kms ⁻¹	-46.3	-60.6	-80.7	-15.8
V kms ⁻¹	-4.1	-21.5	-39.1	-17.5
W kms ⁻¹	-11.9	-8.8	17.9	-48.6
V_{tot} kms ⁻¹	48.0±8.5	64.9±13.9	91.4±2.5	54.0±9.5

Table 3
Equivalent widths for atomic lines

	2M0746	2M1439	2M0036	2M1507
	L0.5	L1	L3.5	L5
LRIS				
K I 7665	9.6±0.5Å	19±0.5Å	<85Å >150Å	
K I 7699	8.8	9.7		
Rb I 7800	2.0	3.0	3.3	6.7
Rb I 7947	3.1	3.0	4.0	7.6
Na I 8183/94	9.1	9.9	7.5	5.1
Cs I 8521	2.7	2.1	2.5	4.6
Cs I 8943	2.2	1.7:	3.6	3.5
HIRES				
H α	1.38±0.05	1.13±0.05		
Ca I 6572	0.69	0.55	0.86	
Li I 6708	<0.2	< 0.05	<0.1	< 0.1
Rb I 7800			4.32	
Rb I 7947		2.0	3.59	4.3
Na I 8183	1.58		2.04	1.39
Na I 8194	3.26		3.76	1.82
8256		0.57	0.57	
Cs I 8521		1.14	2.15	3.44

FIGURE CAPTIONS

Fig. 1.— Far-red optical spectra of the four bright L dwarfs discussed in this paper.

Fig. 2.— Blue/visual LRIS spectra of the 4000 to 7800Å region in late-type dwarfs. In addition to three of the L dwarfs discussed in this paper, we plot spectra for the M9.5 dwarf BRI0021-0214 and for 2MASSWJ150654.4+131206, a bright early-type L dwarf. The more prominent features are identified.

Fig. 3.— Expanded reproductions of the 4500 to 6600Å region of the spectrum for the late-type dwarfs plotted in figure 2, highlighting the strong MgH bands and the substantial increase in strength of the Na D lines.

Fig. 4.— Blue-green spectra of three extreme subdwarfs.

Fig. 5.— The H α region in 2M0746, 2M1439 and 2M0036 from our HIRES observations. The Ca I 6572 absorption is also evident in these spectra, as are TiO bands in the earlier-type dwarfs.

Fig. 6.— The (M_V , (V-I)) and (M_J , (I-J)) diagrams defined by nearby stars with accurate parallax measurements. Crosses mark objects with Hipparcos astrometry; open circles are stars in the 8-parsec sample (Reid & Gizis, 1997) or with ground-based parallax measurements by Monet et al (1992) or Tinney (1996). Note the reversal in (V-I) colour at $M_V > 18$. The four L dwarfs discussed in the present paper are plotted as solid points.

Fig. 7.— High-resolution spectra of the K I 7665/7699 doublet in dwarfs with spectral types between M3 and L4. VB 8 and, to a lesser extent, VB 10 both exhibit chromospheric reversals in the core of both lines.

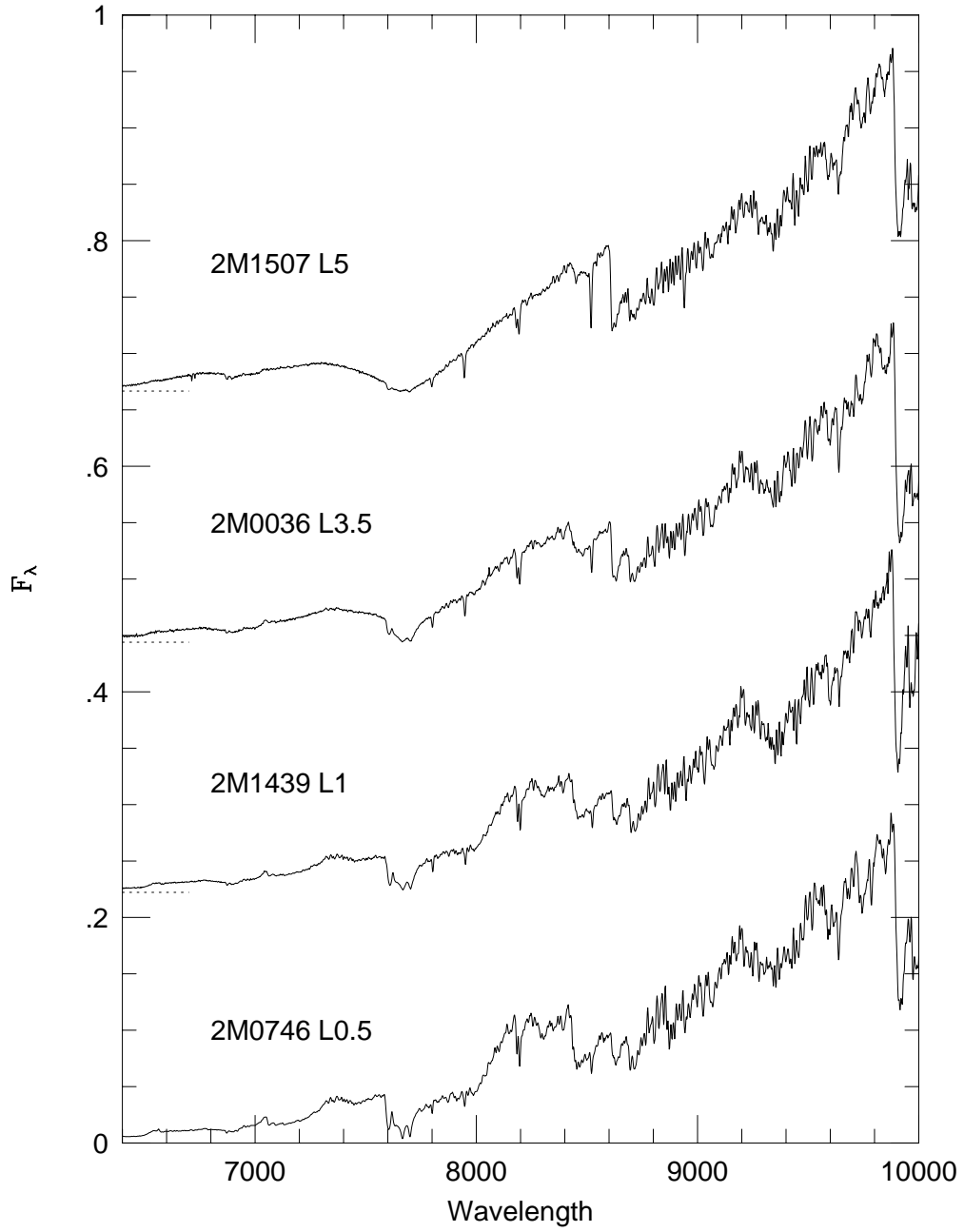


Fig. 1.—

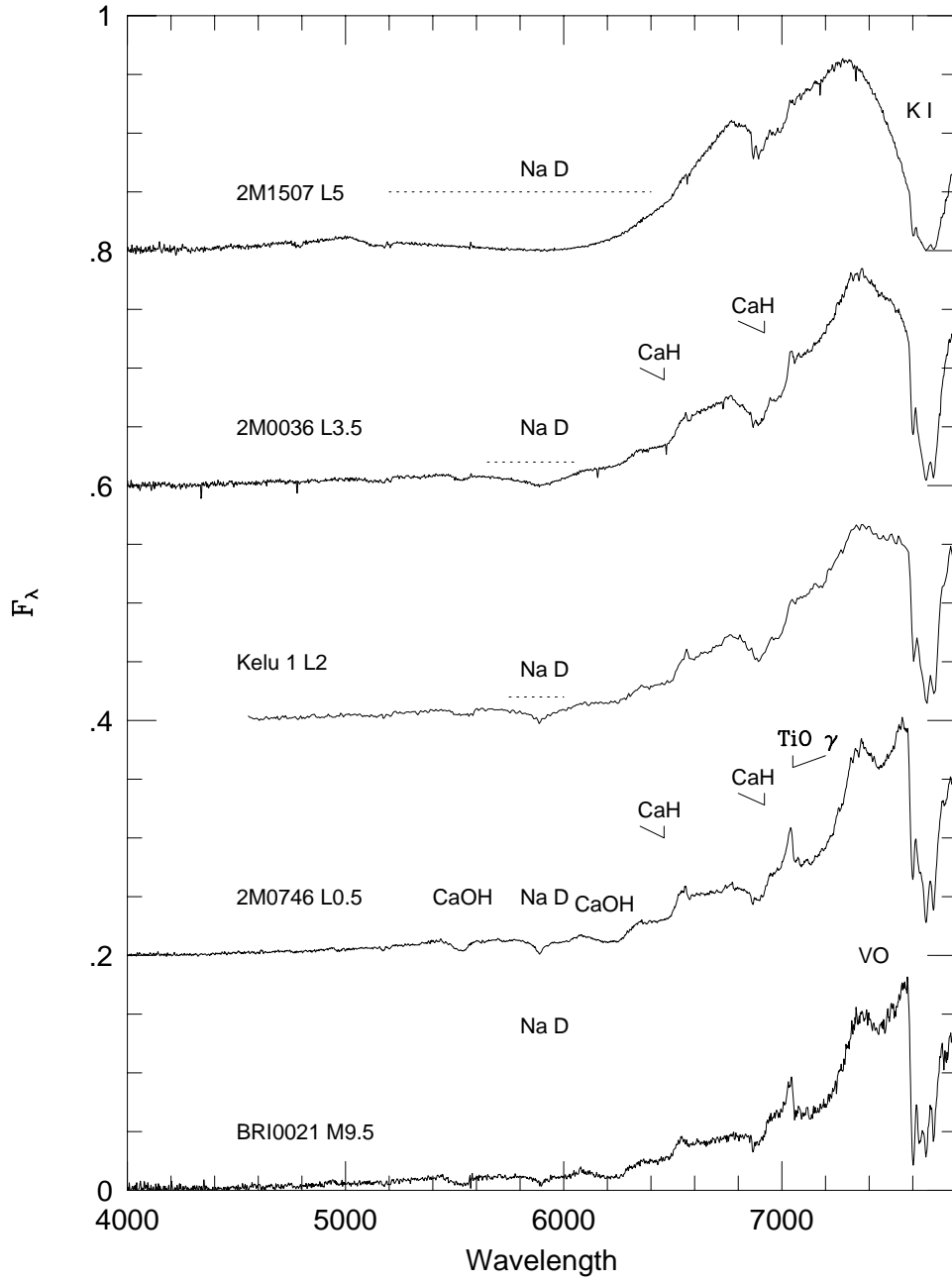


Fig. 2.—

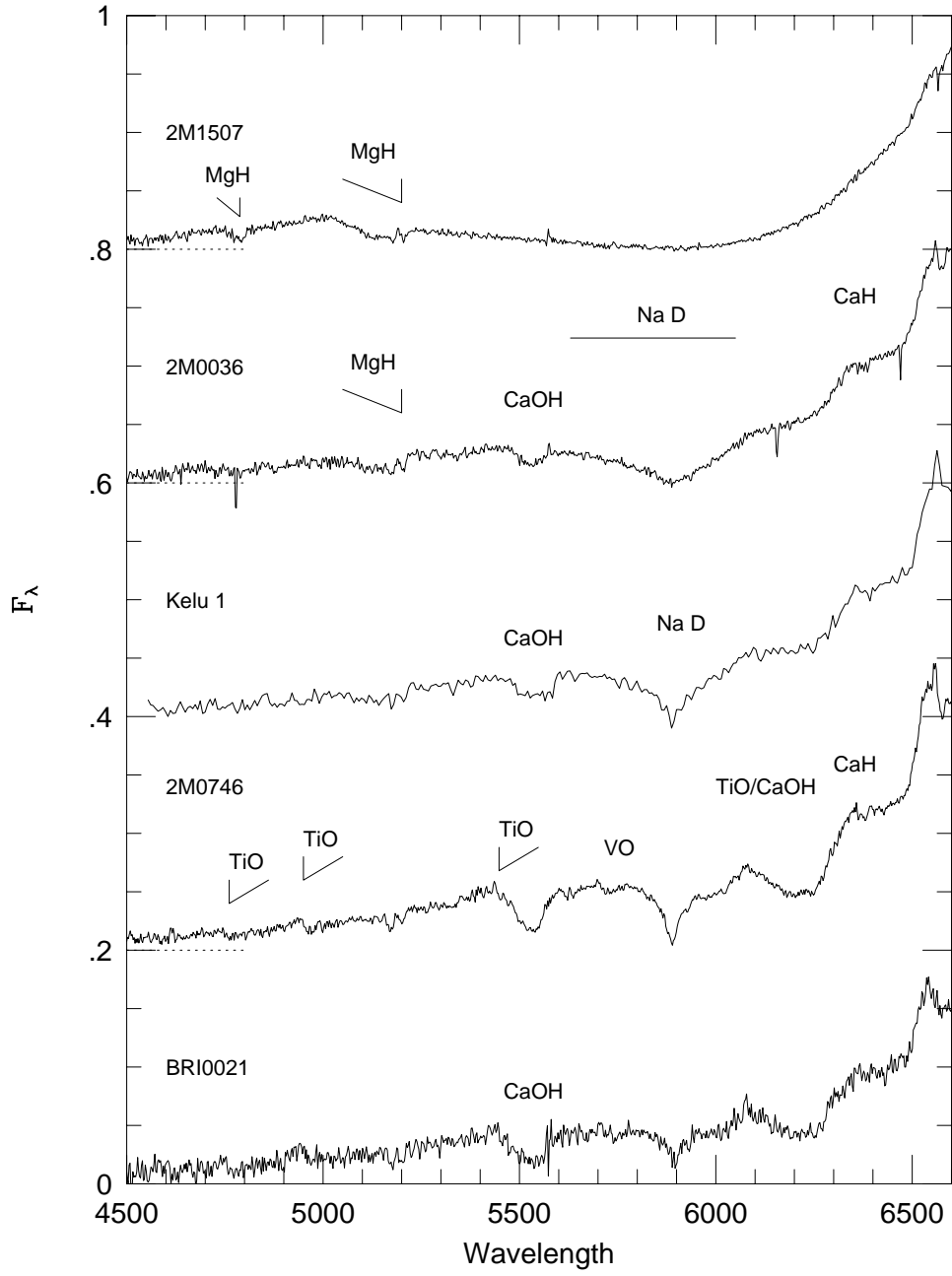


Fig. 3.—

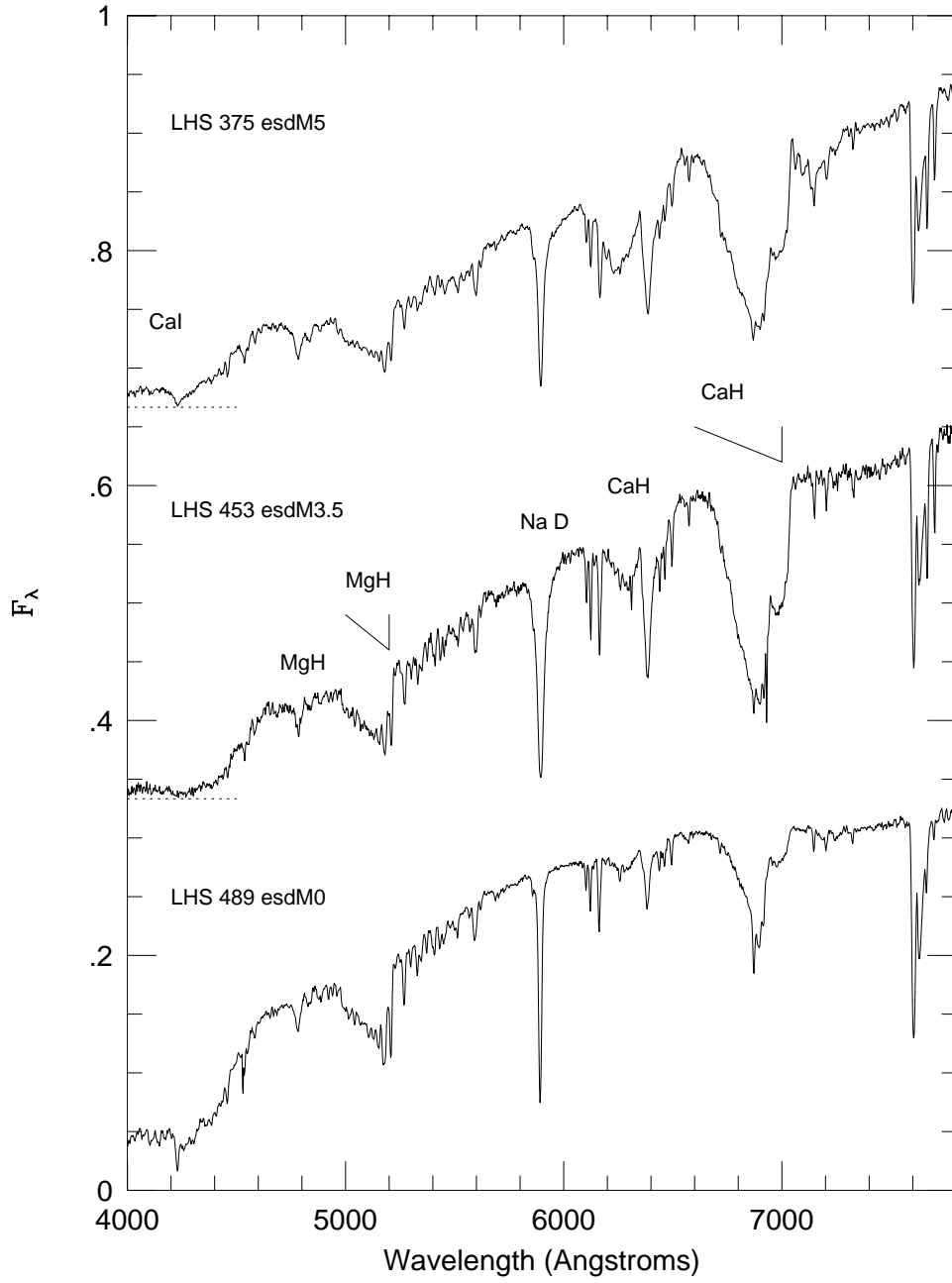


Fig. 4.—

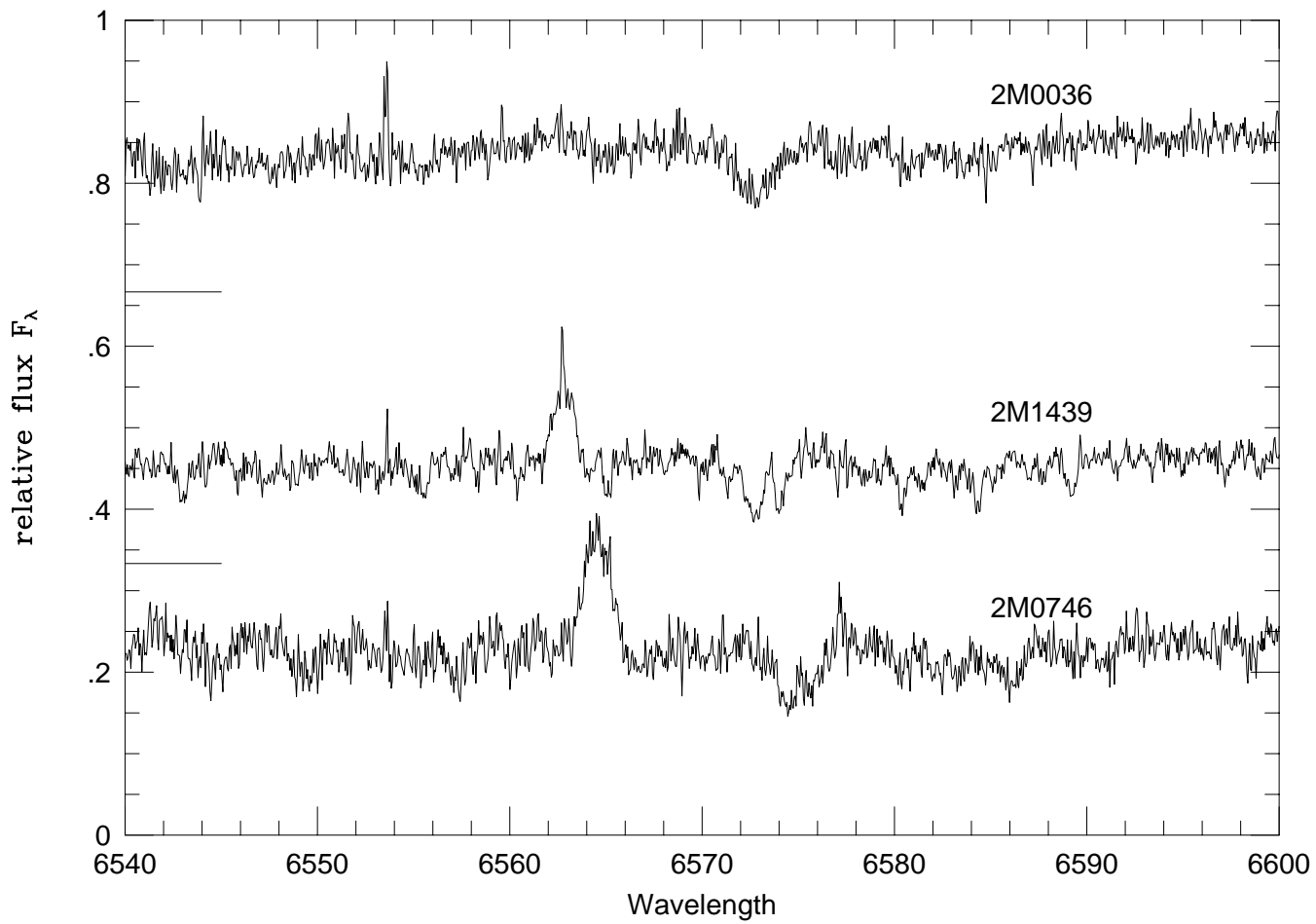


Fig. 5.—

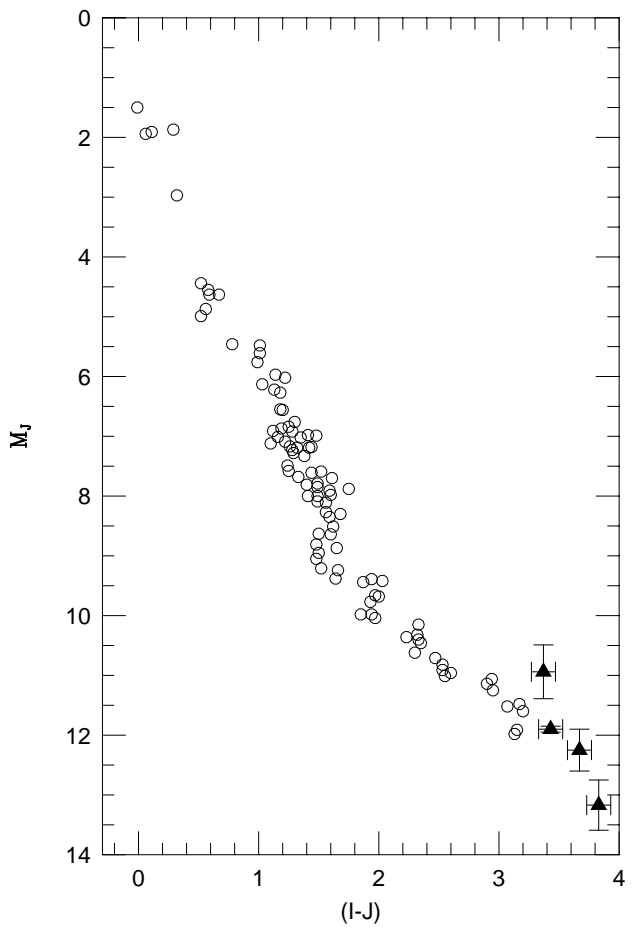
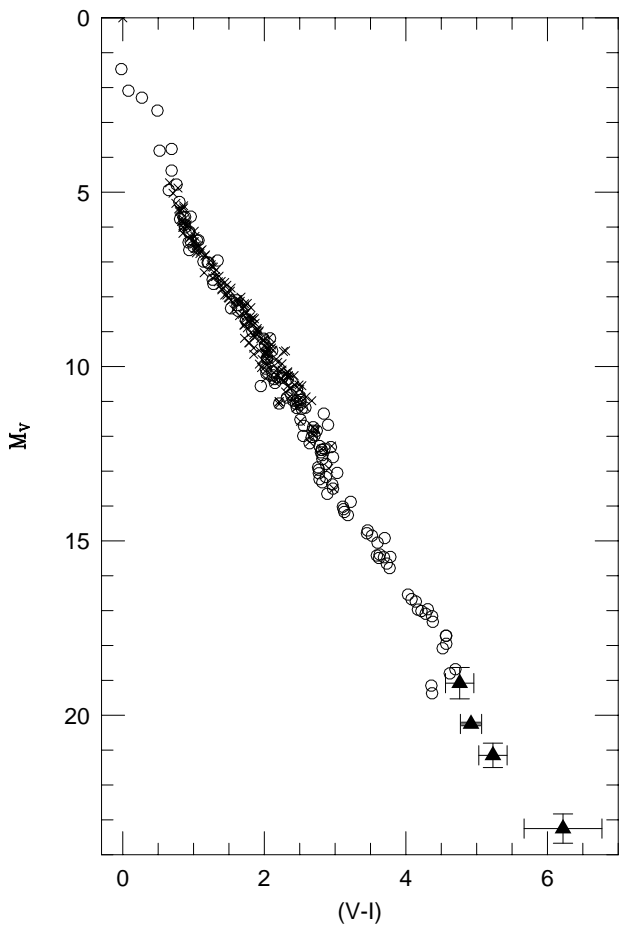


Fig. 6.—

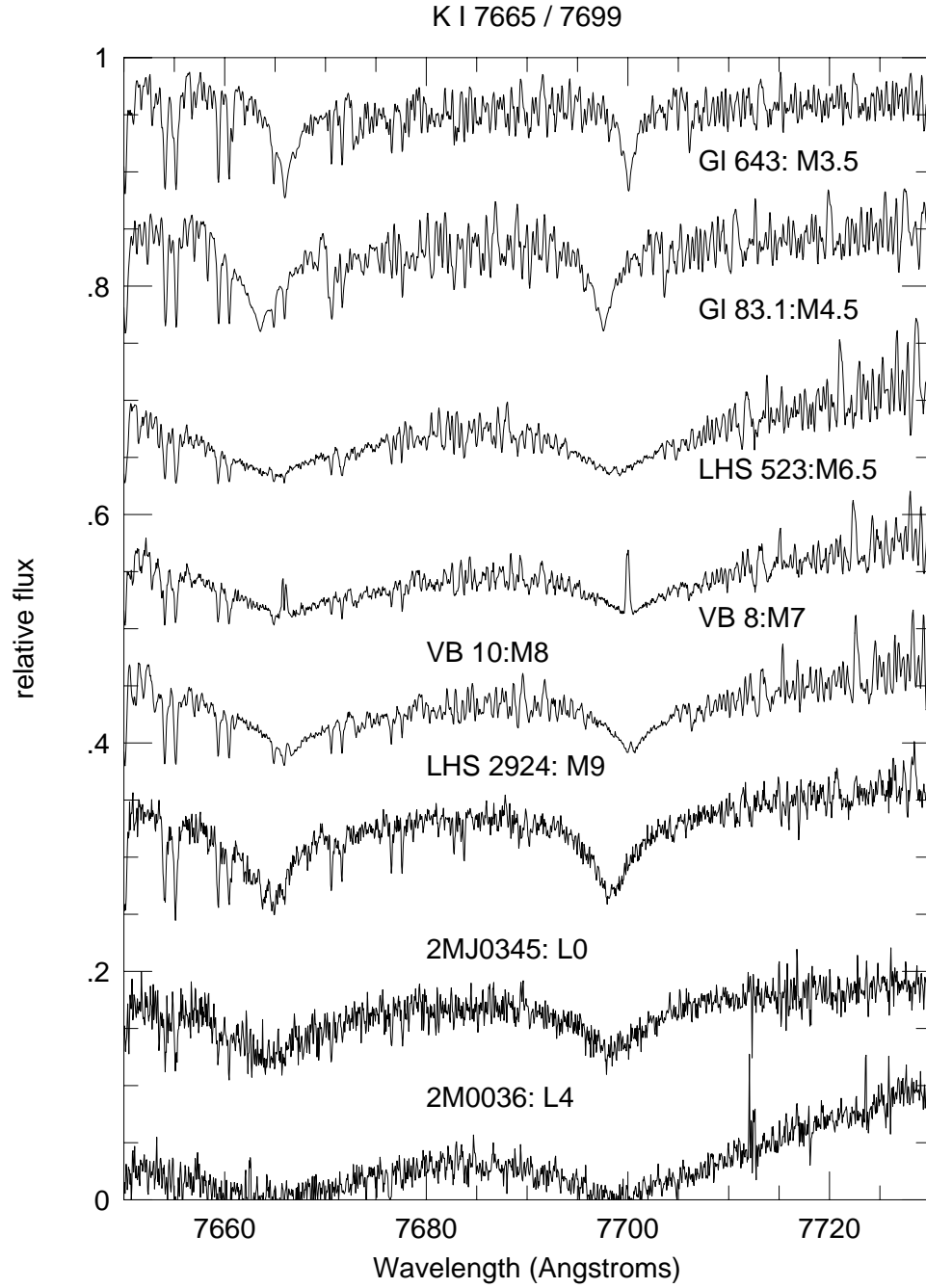


Fig. 7.—